ARTICLE

Carburization of Tungsten Filaments in a Hot-Wire Chemical Vapor Deposition Process using 1,1,3,3-Tetramethyl-1,3-disilacyclobutane

L. Tong and Y. J. Shi*

Department of Chemistry, University of Calgary, Calgary, Alberta T2N 1N4, Canada

ABSTRACT The alloying of tungsten filament when using 1,1,3,3-tetramethyl-1,3-disilacyclobutane (TMDSCB) in a hot-wire chemical vapor deposition reactor was systematically studied by scanning electron microscopy, Auger electron spectroscopy, analysis of the power consumed by the filament, and in situ mass spectrometric measurements of the gas-phase species produced in the process. Only carburization of the W filament was observed. The carburization is mainly caused by the interaction of methyl radicals with the filament. Graphite as well as both WC and W_2C alloys can form on the filament surface, depending on the filament temperatures and source gas pressures. Both WC and graphite are converted to W_2C with the diffusion of C into the filament. It is shown that filament carburization affects the consumption rate of the source gas and the intensities of gas-phase reaction products. Gas-phase reactions dominate at $T \leq 1400$ °C. The carburization rate increases with increasing filament temperatures and dominates at $T \geq 1800$ °C.

KEYWORDS: hot-wire CVD • catalytic CVD • filament aging • carburization • tungsten carbide • 1,1,3,3-tetramethyl-1,3-disilacyclobutane

INTRODUCTION

Since its development in the late 1980s, the technology of hot-wire chemical vapor deposition (HWCVD) (1), also known as catalytic CVD (Cat-CVD) (2), has been successfully used for the deposition of silicon films, silicon alloy films, diamond coatings, and polymer coatings (3). The hot metal filament, usually made of tungsten or tantalum, acts as a catalyzer in dissociating the reactant source gas. It plays an important role in controlling the gas-phase reaction chemistry and, consequently, the film deposition process. It has been demonstrated that exposure of the metal filament to various gas-phase chemical species leads to the formation of filament alloys: for example, metal silicides (4−7) in Si film formation and metal carbides (8−10) in diamond deposition. Filament alloying shortens the filament lifetime (11), changes the radical chemistry on the filament (4, 10), influences the thermal distribution of substrates (11, 12), and affects the deposited film properties (5, 11). All these make the HWCVD process uncontrollable and need to be avoided. Therefore, to achieve a controllable deposition process, it is important to understand the filament alloying process and the formation mechanisms of silicides or carbides.

Recently, our group has studied the formation of tungsten silicides when using silacyclobutane (SCB) as a source gas in a HWCVD reactor (7). It is shown that two phases of tungsten silicide, Si_3W_5 and Si_2W, as well as pure silicon can form depending on the source gas pressures and filament temperatures. The formation of tungsten silicides is mainly due to the production of reactive silylene and silene species from the decomposition of the SCB source gas (13). The formation of silicides when using SCB caused the filament to break and a visible change to occur in the filament appearance. However, when SCB was replaced with 1,1,3,3-tetramethyl-1,3-disilacyclobutane (TMDSCB) molecules in the HWCVD reactor, it was noticed that the filament lifetime has been significantly extended. TMDSCB is a potential single-source organosilane precursor using HWCVD for the formation of amorphous silicon carbide thin films, due to the advantages of reduced decomposition temperatures resulting from the significant ring strain energy in the four-membered-ring structures and the fact that reactive silene and silylene species are produced from the source gas decomposition on the tungsten filament (14). Our study on the gas-phase reaction chemistry of TMDSCB in the HWCVD process (14) indicates that TMDSCB decomposes on the filament to produce methyl and 1,3,3-trimethyl-1,3-disilacyclobutane-1-yl radicals. The dominant secondary gas-phase reactions are the H abstraction reaction from the parent molecule by methyl radicals and subsequent biradical combination reactions. This is quite different from the gas-phase chemistry exhibited by SCB. In order to understand the effect of the gas-phase chemistry on the filament aging and vice versa, it is necessary to systematically study the filament aging process when using TMDSCB as a source gas.

In this work, aged tungsten filament samples were carefully prepared by exposure to TMDSCB molecules of different partial pressures at different filament temperatures. The morphology and chemical composition of the aged filaments were examined by scanning electron microscopy (SEM) and Auger electron spectroscopy (AES), respectively. The power supplied to the filament was monitored in the aging process

* To whom correspondence should be addressed. E-mail: shiy@ucalgary.ca.

Received for review May 14, 2009 and accepted August 17, 2009

DOI: 10.1021/am900329q

© 2009 American Chemical Society

to illustrate the changes in the filament properties caused by alloying. Detection of the gas-phase chemical species produced during the preparation of each aged filament were also made in situ using a time-of-flight (TOF) mass spectrometer coupled with a nonresonant single photon ionization (SPI) with a 10.5 eV vacuum ultraviolet (VUV) laser radiation. This serves to give us some insight into the relationship between the gas-phase chemistry and filament alloy formation.

EXPERIMENTAL SECTION

The aged W filaments were prepared in a HWCVD reactor by exposure to TMDSCB samples of different pressures and at different filament temperatures. Details of the HWCVD reactor have been described previously (13, 15). Briefly, the reactor is a cylindrical stainless steel chamber (volume 7.1 L) housing a straight W wire (99.9%, Aldrich) with a diameter of 0.5 mm and a length of 10 cm. The filament was resistively heated by a dc power supply, and its temperature was measured by a two-color IR pyrometer (Chino Works) through an optical window. The TMDSCB/He samples were introduced into the reactor through a $^1/_4$ in. diameter stainless steel tube. The gas flow rate was controlled by a mass flow controller (MKS, type 1179A) to maintain a constant pressure of 12 Torr in the reactor. The typical gas flow rate was 0.70 sccm. The pressure was monitored by a capacitance manometer (MKS, type 626A). Three different concentrations of the TMDSCB/He mixture at 1%, 2%, and 4% were used in this work. The TMDSCB (97%, Starfire Systems) sample was first degassed using several freeze−pump−thaw cycles. The room-temperature vapor of TMDSCB was then entrained in helium (99.995%, Praxair) in a 2.25 L stainless steel sample cylinder to give a mixture. By using the 1%, 2%, and 4% of TMDSCB/He samples, the partial pressures of TMDSCB in the reactor are 0.12, 0.24, and 0.48 Torr, respectively.

After each new filament was placed in the reactor, it was heated to 2000 °C in 12 Torr of 1% H_2 in He for 2 h. This serves to clean the chamber wall from any deposits from previous deposition runs and to set the filament conditions the same before it is aged. The filament was then exposed to each of the three TMDSCB samples for 1 h at each different temperature. Filament temperatures between 900 and 2000 °C with an increment of 100 °C were studied. During the 1 h aging, the filament temperature was kept constant by adjusting the power supplied to the filament. At the end of the 1 h run, the filament was removed from the reactor and stored under vacuum before being subjected to the characterization using SEM (Philips XL30, operating at 20.0 kV) and AES. The AES measurements were carried out using a JAMP-9500 F Auger microprobe (JEOL) with a 7.5 nm resolution at an accelerating voltage and emission current of 15.0 kV and 10 nA, respectively. The filament samples were sputtered for 30 s using an Ar^+ beam (30 kV and 30 μA) before taking the AES measurements.

The gas-phase chemical species formed in the reactor during the 1 h aging process was monitored by 10.5 eV VUV SPI/TOF MS. Details of the experimental setup to record the VUV laser SPI TOF mass spectra of gas-phase species can also be found in our previous publications (13, 15). Only the essential features are described here. The HWCVD reactor connects through a pinhole of 0.15 mm diameter to the main ionization/detection chamber housing a linear TOF mass spectrometer. The ionization wavelength at 118 nm was produced by frequency-tripling of the 355 nm UV output (20 mJ/pulse, 10 Hz) from a Nd:YAG laser (Spectra-Physics, LAB-170-10) in a gas cell containing 190 Torr of a phase-matched 10:1 Ar−Xe gas mixture. Signals from the microchannel plate (MCP) detector in the TOF mass spectrometer were preamplified, displayed on a 300 MHz digital oscilloscope (Tektronix, TDS3032B), and saved in a computer using an e-scope for analysis. The mass spectra were taken every 5 min after the filament was turned on at each temperature for 1 h.

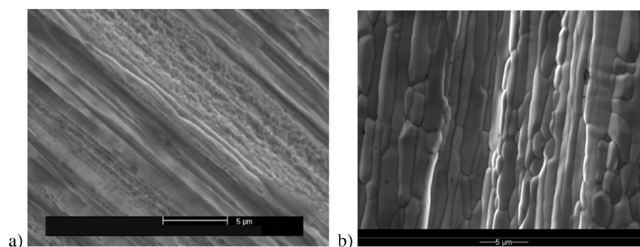

FIGURE 1. SEM images of (a) a new W filament without any treatment and (b) a W filament after being heated to 2000 °C in 12 Torr of 1% H_2 in He for 2 h.

RESULTS AND DISCUSSION

1. Carburization of Filaments. To study the effect of source gas pressures and filament temperatures on the filament alloying, 36 aged filaments were carefully prepared by exposure to TMDSCB with three different pressures (i.e., 0.12, 0.24, and 0.48 Torr) at different temperatures ranging from 900 to 2000 °C with an increment of 100 °C. The surface morphology of all 36 filaments was studied by SEM. For comparison, the SEM images of a new W filament without any treatment and a W filament after being heated to 2000 °C in 12 Torr of 1% H_2 in He for 2 h were also taken, and they are shown in Figure 1. Examination of the SEM images of all 36 filaments showed that the morphology of the filaments exposed to low filament temperatures at 900 and 1000 °C for all three samples with different TMDSCB pressures resembled closely that of the filament after heat treatment in H_2. A representative image from the filament exposed to 0.24 Torr of TMDSCB at 1000 °C is shown in Figure 2a. For filaments exposed to 0.48 Torr of TMDSCB, the morphology started to change when the temperature was further increased to 1100 °C, as shown in Figure 2b.

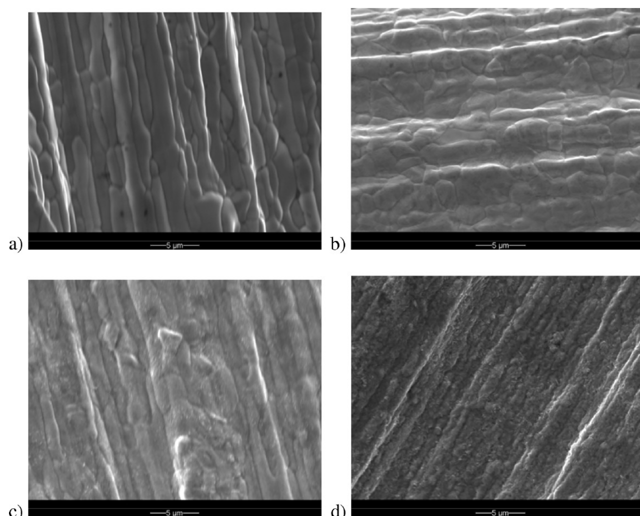

FIGURE 2. SEM images of the W filament exposed to (a) 0.24 Torr of TMDSCB at 1000 °C, (b) 0.48 Torr of TMDSCB at 1100 °C, (c) 0.24 Torr of TMDSCB at 1200 °C, and (d) 0.12 Torr of TMDSCB at 1300 °C.

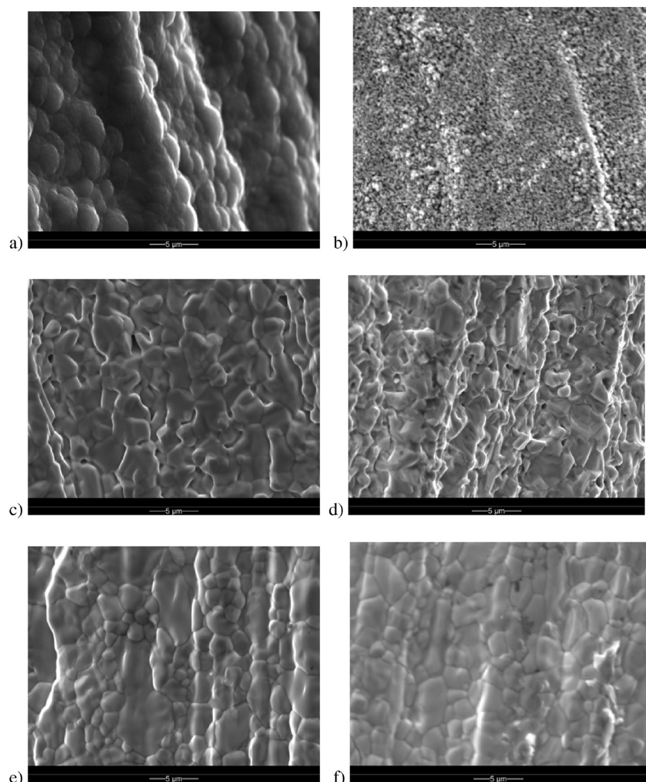

FIGURE 3. SEM images of the W filament exposed to (a) 0.48 Torr of TMDSCB at 1700 °C, (b) 0.24 Torr of TMDSCB at 1700 °C, (c) 0.12 Torr of TMDSCB at 1700 °C, (d) 0.48 Torr of TMDSCB at 2000 °C, (e) 0.24 Torr of TMDSCB at 2000 °C, and (f) 0.12 Torr of TMDSCB at 2000 °C.

This indicates that deposits started to form on the W filament at this temperature if 0.48 Torr of TMDSCB gas was used. It was found that the temperature at which a change in the morphology was first observed increased to 1200 and 1300 °C, respectively, for filaments exposed to samples with lower pressures of TMDSCB at 0.24 and 0.12 Torr. The SEM images of the two filaments prepared at 1200 °C with 0.24 Torr of TMDSCB and at 1300 °C with 0.12 of Torr TMDSCB, shown in Figure 2c,d, respectively, illustrated clearly the change. This suggests that with increasing source gas pressures in the reactor the deposits started to form at lower filament temperatures. From our in situ monitoring of the parent ion intensity in the mass spectra, it is found that the amount of TMDSCB consumed in the 1 h time period for one temperature always increases with increasing initial source gas pressures. With more TMDSCB molecules consumed when using higher pressure samples, the temperature for the deposits on the filament to appear was lowered. At temperatures higher than 1300 °C, there are significant changes in the surface morphology. For example, Figure 3a−c shows the images from filaments exposed to TMDSCB samples at three different pressures but at the one same temperature of 1700 °C. These three images are representative of those prepared at filament temperatures of 1400−1700 °C at each different pressure. At even higher temperatures of 1800−2000 °C, the surface morphologies are different from those at 1400−1700 °C on comparison of images of filaments exposed to the same sample. This is illustrated in the representative SEM images from the filaments prepared at 2000 °C with 0.48, 0.24, and 0.12 Torr of TMDSCB, respectively, shown in Figure 3d−f.

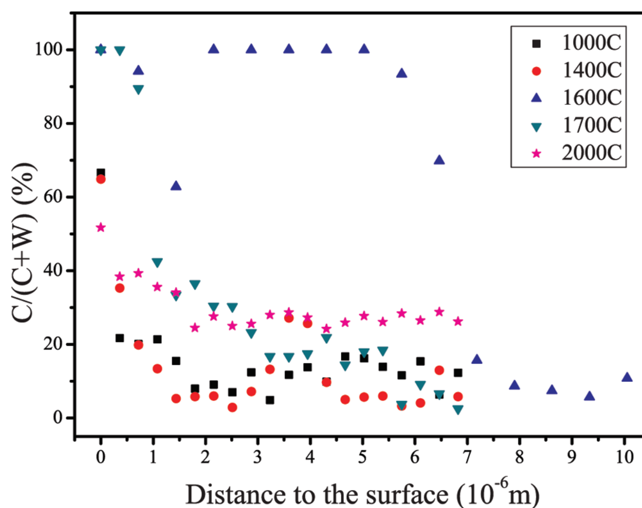

FIGURE 4. Carbon content (C/(C + W)) in percentage as a function of the distance to the filament surface for filaments exposed to 0.48 Torr of TMDSCB at 1000, 1400, 1600, 1700, and 2000 °C.

AES measurements were made to determine the chemical composition of the deposits on the W filament. The filaments prepared at five temperatures, i.e., 1000, 1400, 1600, 1700, and 2000 °C, exposed to each of the three different TMDSCB samples were examined. The AES measurements were performed at the filament surface and at different depths into the interior of the filaments. No signals from silicon were detected in any of the 15 filaments tested. Only carbon and tungsten signals were observed. Figure 4 shows the depth profile of the carbon content (C/(C + W)) in percent for the filaments exposed to 0.48 Torr of TMDSCB at the five different temperatures. The carbon content in the W filament after heat treatment in 12 Torr of 1% H_2 in He at 2000 °C for 2 h was determined to be 1.4 ± 0.4% from an AES measurement from the filament surface to 6.0 μm toward the filament center. Therefore, it is clear from Figure 4 that there is an increase in C content both on the surface and toward the interior when the filaments were exposed to TMDSCB molecules. The surface C contents maximized to 100% at 1600 and 1700 °C, representing a pure graphite layer. At both lower and higher temperatures, the surface C contents were reduced to 66.6%, 64.9%, and 51.7%, respectively, for 1000, 1400, and 2000 °C. According to the phase diagram of C−W (16, 17), two phases of tungsten carbide, W_2C (β'') and WC (δ), can form at temperatures lower than 2000 °C. The abundances of W, W_2C, WC, and C in the two-phase equilibrium leading to different surface C contents are given in Table 1. The surface C contents for the other 10 filaments and the corresponding composition of 2 phases in equilibrium can be found in the same table. Depending on the temperatures and source gas pressures at which the filaments were prepared, graphite as well as both tungsten carbide (WC) and subcarbide (W_2C) can be formed on the surface. It is clear from Table 1 that an increase in the source gas pressure caused an increase in surface C content at a fixed filament temperature. The only exception is 1400 °C, which cannot be explained. When the

ARTICLE

Table 1. Surface C Contents of Aged Filaments Determined by AES Measurements and the Corresponding Abundances of the Two Phases in Equilibrium

filament	pressure[a] (Torr)	temp[b] (°C)	C/(C + W) (%)	abundance (%) C	WC	W_2C	W
A	0.12	1000	10.5	0	21.0	0	79.0
B	0.24	1000	39.1	0	78.2	0	21.8
C	0.48	1000	66.6	33.2	66.8	0	0
D	0.12	1400	58.9[c,f]	17.8	82.2	0	0
E	0.24	1400	91.0	82.0	18.0	0	0
F	0.48	1400	64.9	29.8	70.2	0	0
G	0.12	1600	46.4[d,f]	0	78.4	21.6	0
H	0.24	1600	100	100	0	0	0
I	0.48	1600	100	100	0	0	0
J	0.12	1700	39.9[d,f]	0	39.4	60.6	0
K	0.24	1700	97.5	95.0	5.0	0	0
L	0.48	1700	100	100	0	0	0
M	0.12	2000	24.3[d,g]	0	0	81.5	18.5
N	0.24	2000	41.2[e,g]	0	47.2	52.8	0
O	0.48	2000	51.7	3.4	96.6	0	0

[a] Partial pressure of TMDSCB in the reactor. [b] Filament temperature. [c] Measurement taken at 0.09 μm. [d] Measurements taken at 0.18 μm. [e] Measurement taken at 0.36 μm from the surface. All other measurements were taken at 0 μm from the surface. [f] Fitting of the depth profile for filaments D, G, and J gives surface C contents of 63.6%, 60.2%, and 49.9%, respectively. [g] The average C contents from 0−7 μm depth for filaments M and N are 23.1% and 33.1%, respectively.

filaments were exposed to source gases of the same pressures, the surface content first increased with increasing temperature but decreased at higher temperatures. This is due to a competition between gas-phase reactions and the filament carburization and/or C diffusion into W filament, which will be discussed in detail later. The optimum temperatures for the surface C contents from filaments prepared with 0.24 and 0.48 Torr of TMDSCB were determined to be 1600−1700 °C. With 0.12 Torr of TMDSCB, the optimum temperature was at 1400 °C.

As shown in Figure 4 for filaments exposed to 0.48 Torr of TMDSCB, at all filament temperatures the C content decreased with increasing depth into the interior of the filaments and each reached a relatively constant level of C content. For the filament exposed to 1600 °C, the C content did not show a decrease until after 5 μm into the W filament, indicating a carbonaceous layer on the surface. This suggests that the diffusion rate of C into the W filament is low at this temperature and it cannot catch up with the growth of the carbonaceous layer. It is interesting to find that the terminal levels of C content all fell into a region below 33%, no matter how high the surface C content was to start with. This is also true for the filaments prepared with two other TMDSCB samples with partial pressures of 0.24 and 0.12 Torr, as shown in Figure 5a,b, respectively. Therefore, when C diffuses into the W filament, both WC and graphite are converted to W_2C. This is in agreement with a previous study by Okoli et al. (18), where the W_2C layer growth was found to be the dominant carbide growth at 2000 °C when using either 0.5% or 1.0% CH_4 in H_2 with a total pressure of 10 or 40 Torr. In the study by Zeiler et al. on the structural changes of W filaments during HWCVD of diamond (9), it was found that W (0.5 mm diameter) was transformed completely into W_2C 70 min after the filament was exposed to 22.5 Torr of 1% CH_4 in H_2 at an initial temperature of 2450 °C. A WC shell started to grow from the outside surface slowly and was not completed after 4 h. In our work, after the W filament was exposed to 0.48 Torr of TMDSCB for 1 h at 2000 °C (filament O), the thickness of the W_2C layer was found to be 47 μm, as shown in the cross-sectional SEM images in Figure 6a. This only covers about 9% of the whole cross-section length of the W filament, indicating that the carburization of W filaments in our work is slower in than those by Zeiler et al. This is mainly due to the lower temperatures used in our work. Examination of the cross-section SEM images of all 12 filaments exposed to 0.48 Torr of TMDSCB samples confirmed that an increase in temperature significantly increases the W_2C layer thickness, as is shown in the cross-sectional SEM images of the filaments exposed to the same TMDSCB sample but at lower temperatures of 1900−1700 °C in Figure 6b−d. A clear change in the cross-sectional images was observed when the temperature was changed from 1700 to 1800 °C, which coincided with an obvious change of the surface SEM images with the specified temperature change. The increase in the carburization rate with

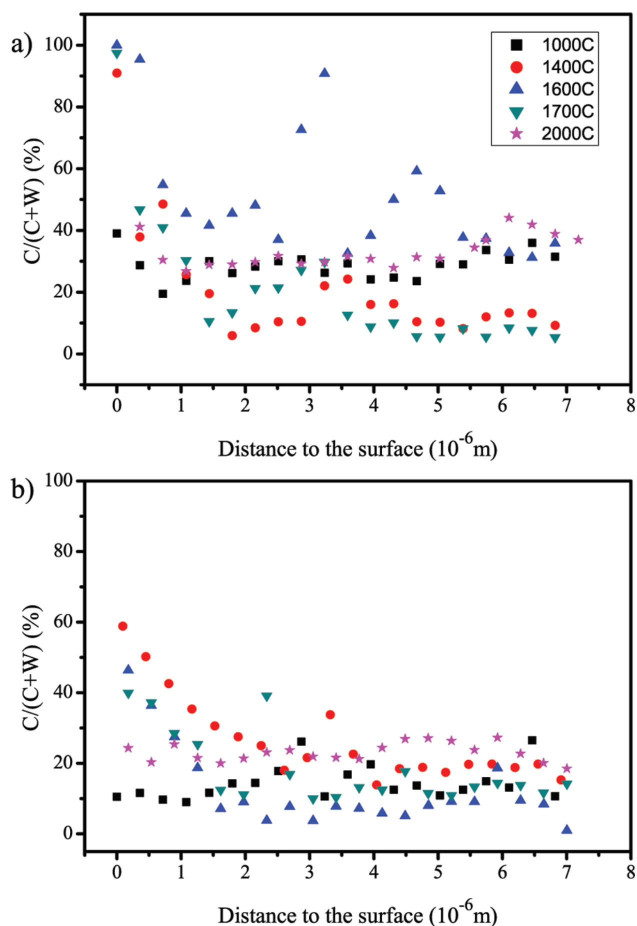

FIGURE 5. Carbon content (C/(C + W)) in percent as a function of the distance to the filament surface for filaments exposed to (a) 0.24 Torr and (b) 0.12 Torr of TMDSCB at 1000, 1400, 1600, 1700, and 2000 °C.

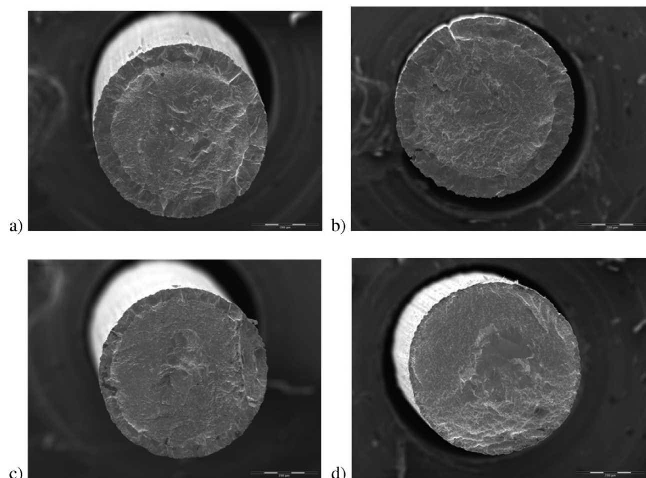
FIGURE 6. Cross-sectional SEM images of W filaments exposed to 0.48 Torr of TMDSCB for 1 h at (a) 2000 °C, (b) 1900 °C, (c) 1800 °C, and (d) 1700 °C.

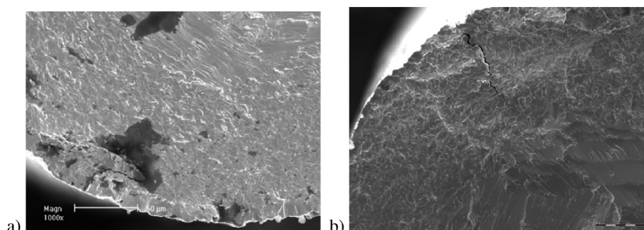
FIGURE 7. Cross-sectional SEM images of W filaments exposed at 2000 °C for 1 h to (a) 0.24 Torr and (b) 0.12 Torr of TMDSCB.

increasing temperature when using TMDSCB source gas can be explained by an increase in the diffusion rate when the temperature is increased (4, 8). In a study on the formation of tungsten silicides during Si film formation using SiH_4, Honda et al. (6) reported that the thickness of the silicide layer increased with temperature when it was lower than 1650 °C but started to decrease with temperature when it was higher than 1750 °C. They attributed this to a competition between the formation of silicides and the thermal desorption of Si atoms from the filament surface. Our results suggest that, at temperatures lower than 2000 °C, the evaporation of C from the filament surface is not significant and carburization dominates, leading to an increase in the W_2C layer thickness. The cross-section images of the filaments prepared at 2000 °C for 1 h with TMDSCB at 0.24 Torr (filament N) and 0.12 Torr (filament M) are shown in Figure 7. The W_2C layer thicknesses for filaments N and M were determined to be 14 and 11 μm, respectively. Comparison to the layer thickness of 47 μm for filament O clearly indicates that increasing the TMDSCB pressure leads to a significant increase in the W_2C layer thickness.

2. Power Consumption by the Filaments. During the 1 h filament carburization process, constant filament temperatures were maintained by adjusting the dc power supplied to the filament. Recently, there has been increasing interest in understanding the power consumption in the HWCVD process (6, 9, 10, 19−21). The power consumed is now well described by eq 1.

$$P = P_{rad} + P_{conv} + P_{cond} + P_{re} \tag{1}$$

Here P_{rad} is the power loss by radiation, P_{conv} is the loss by convection of surrounding gases, P_{cond} is the loss by heat conduction via the clampings, and P_{re} is the power consumed in the chemical reactions on the filament surface. Figure 8 shows the power consumption data for a W filament under vacuum and in 12 Torr of He gas. The filament was heated for 2 h in a 12 Torr 1% H_2 in He sample. The power supplied to the filament under vacuum is in a linear relationship with T^4, which agrees with previous studies that the dominant power loss mechanism under vacuum is radiation with its power described by the Stefan−Boltzmann equation:

$$P_{rad} = \varepsilon\sigma T^4 S \tag{2}$$

where $\sigma = 5.67 \times 10^{-12}$ W cm^{-2} K^{-4} is the Stefan−Boltzmann constant, ϵ is the emissivity, and S is the surface area of the filament. Assuming a filament length of 10 cm, the power data under vacuum shown in Figure 8 give an effective emissivity of W of 0.18. The difference between the power dissipation in He and that under vacuum is due to convection by the He gas. In our experiments, the pressure in the chamber was maintained at 12 Torr; as a result, the power loss by convection should not change much. As demonstrated by previous studies (6, 9), the energy transport by conduction is insignificant. Therefore, the change in the supplied power during the carburization process is mainly due to the power loss by either radiation or chemical reactions. Figure 9 shows the plots of supplied power versus the filament-on time during the 1 h period to maintain a filament temperature at 1000 °C for three different TMDSCB samples. For all power plots shown in Figure 9 and those at other temperatures, there is usually an initial increase, be it large or small. This resulted from the energy loss due to the dissociation of TMDSCB on the filament, as was also seen when using SiH_4 (6). In a previous

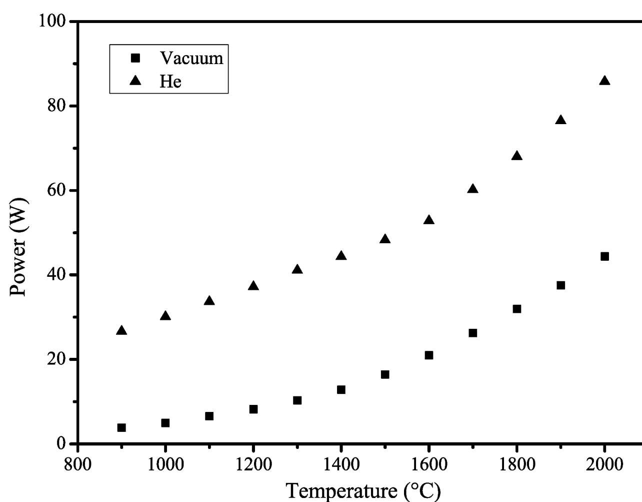

FIGURE 8. Relation between filament temperature and power consumed under vacuum (■) and in 12 Torr of He (▲).

ARTICLE

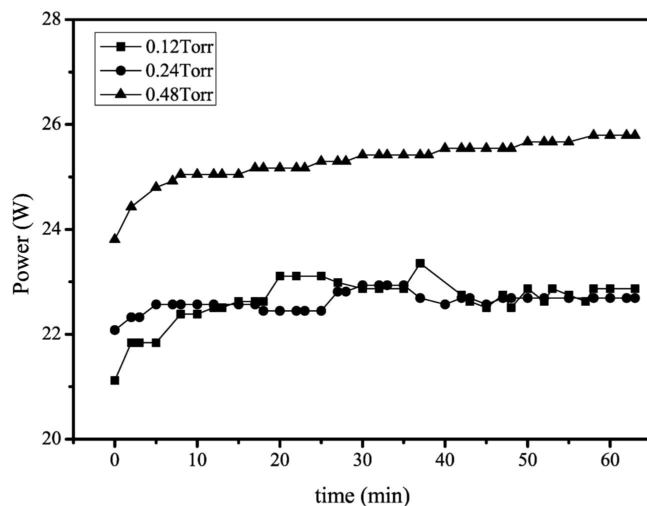

FIGURE 9. dc electric power during the 1 h filament carburization process to maintain a filament temperature at 1000 °C for three different TMDSCB samples: (■) 0.12 Torr; (●) 0.24 Torr; (▲) 0.48 Torr.

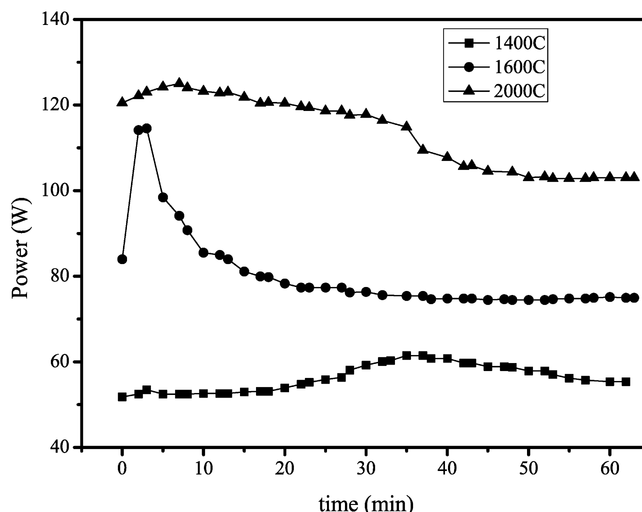

FIGURE 10. dc electric power during the 1 h filament carburization process using the TMDSCB sample of a partial pressure of 0.48 Torr to maintain filament temperatures at 1400 °C (■), 1600 °C (●), and 2000 °C (▲).

study by Comerford et al. (10), it was found that the power changed little during the 7.75 h carburization process using CH_4/H_2 mixtures. The steady-state power after the initial increase in our study should also correspond to the carburization stage. At a low temperature of 1000 °C, only WC and C phases can be formed. From Table 1, it is clear that the surface of the filament exposed to 0.48 Torr of a TMDSCB sample was covered by both graphite and WC, whereas only WC covered the surfaces of the filaments exposed to lower pressures of TMDSCB vapors. The higher emissivity of graphite ($\epsilon \approx 0.95$ (10)) relative to that of tungsten carbide (ϵ (WC) = 0.3−0.76 (22)) causes an increased power loss via radiation. This explained the power profile at 1000 °C shown in Figure 9. When the temperature was increased to above 1250 °C, tungsten subcarbide (W_2C) was formed in addition to WC and C. As mentioned previously in the AES depth profile, no matter which phase was formed on the surface, with the diffusion of C into the W filament, both WC and C could be converted to W_2C. A decrease in power with time after the initial increase was observed from the power profiles for $T \geq 1300$ °C. The plots of supplied power versus the filament-on time during the 1 h carburization exposed to the 0.48 Torr TMDSCB sample to maintain filament temperatures at 1400, 1600, and 2000 °C shown in Figure 10 illustrates this trend. This suggests that the emissivity of W_2C is smaller than that of WC, which is confirmed by the reported value of 0.25−0.40 for W_2C (22). The power consumption data recorded in our study shows that the emissivity change due to filament carburization is the dominant mechanism controlling the change in the power. This supports previous results that the emissivity change is the main reason there is a power increase to maintain a constant temperature (10) or a temperature drop when the power is kept constant (6, 18).

3. Effect of Filament Carburization on the Gas-Phase Chemistry. In this work, when the TMDSCB molecule containing both Si and C was used in the HWCVD reactor, it was found that only carburization of the W filament occurred in the HWCVD reactor and silicidation was not observed. As has been demonstrated in our previous work (14) on gas-phase reaction chemistry with TMDSCB, the molecule decomposes on the hot W filament to CH_3 and 1,3,3-trimethyl-1,3-disilacyclobutan-1-yl radicals. The dominant secondary reaction pathways in the reactor are the hydrogen abstraction reactions from the parent TMDSCB molecule by methyl radicals and subsequent biradical combination reactions. The CH_3 radical has long been viewed as the dominant growth precursor for diamond deposition (23−25). The carburization of tungsten filaments is known to occur during diamond deposition by hot filament assisted CVD using CH_4/H_2 gas mixtures (9, 10, 18). Winters et al. (26−28) have shown that the reaction probability of methane with tungsten is quite small. The carburization of a tungsten filament in a typical diamond CVD reactor is mainly due to its reactions with methyl radicals, ethylene, and acetylene that are generated by atomic hydrogen from the H_2 decomposition on the hot filament with methane. Our observations that only filament carburization occurs when using TMDSCB and the generation of CH_3 radical from the primary decomposition on the filament as well as its dominant involvement in the secondary gas-phase reactions in the reactor agree well with the results assumed by the diamond deposition processes.

To study the interplay of filament carburization and gas-phase chemistry, we have monitored the intensity change of the gas-phase reaction products in situ during the 1 h filament carburization process using a mass spectrometer coupled with a VUV ionization laser source. In our experiments, the TMDSCB/He samples were continuously flown into the reactor and pumped through a 0.15 mm diameter pinhole to the main vacuum chamber. The residence time, τ_r, for a molecule in the reactor at a room temperature of 20 °C is given by (29)

$$\tau_r = 73.6\frac{PV}{Q} \qquad (3)$$

where Q is the flow rate in sccm, P is the pressure in the reactor in Torr, and V is the reactor volume in liters. Given a total pressure of 12 Torr and a flow rate of 0.70 sccm, the residence time of the sample molecules in our experiments is 149 min. Our previous work (14) has shown that the leading gas-phase product from the dominant secondary reaction pathways involving mainly methyl radicals and the parent molecules was 1,3,3-trimethyl-1-ethyl-1,3-disilacyclobutane with a mass of 158 amu. Figure 11 shows the intensity distribution curves versus the filament-on time for the signals from the 1,3,3-trimethyl-1-ethyl-1,3-disilacyclobutane ion for each of the three TMDSCB samples with a partial pressure of 0.12, 0.24, and 0.48 Torr at different filament temperatures. To avoid congestion, only the intensity data for six temperatures at 1300, 1400, 1600, 1700, 1800, and 2000 °C are shown in Figure 11. For all three samples, the intensity of the peak at *m/z* 158 was very weak at temperatures lower than 1200 °C. When the temperature was increased to 1300 and 1400 °C, the increase in the peak intensity was more obvious. Although more 1,3,3-trimethyl-1-ethyl-1,3-disilacyclobutane molecules were produced when using more TMDSCB in the reactor, a steady state was reached for all three samples at the two temperatures. At 1600 and 1700 °C, the peak intensity first increased with time but decreased later in the 1 h run. This results from the competition between the gas-phase reactions, leading to the formation of 1,3,3-trimethyl-1-ethyl-1,3-disilacyclobutane and the effect of the carburized filament on the reaction rate. At the beginning, the reactions are fast, causing an increase in the peak intensity at *m/z* 158. However, when the filaments were carburized, this slowed down the reactions and the intensity showed a decrease. It could be argued that the decrease in the intensity of the peak at *m/z* 158 was due to its involvement in the secondary reactions, leading to high-mass species such as 1,3-dimethyl-1,3-diethyl-1,3-disilacyclobutane (*m/z* 172), 3-methyl-1,1,3-triethyl-1,3-disilacyclobutane (*m/z* 186), etc. (14). If this is true, the intensities of the peaks at *m/z* 172 and 186 are expected to increase with time at 1600 and 1700 °C. Examination of the intensity profile of these two peaks showed a similar trend to that at *m/z* 158: i.e., they reached optimum intensities after the filament was turned on for 20−25 and 5 min, respectively, for the TMDSCB samples with a partial pressure of 0.24 and 0.48 Torr. Therefore, the contribution from the consumption of 1,3,3-trimethyl-1-ethyl-1,3-disilacyclobutane (*m/z* 158) in the secondary gas-phase reactions to the decrease of the peak intensity can be discounted. The intensity decrease at a later time in the run is mainly due to the carburization of the filament. With further increase of temperatures to 1800 and 2000 °C, the decrease in the peak intensity at *m/z* 158 became more significant. This is accompanied by an equally dramatic change in the intensity of the parent ion at *m/z* 144. The intensity profile of the peak at *m/z* 144 showed that a complete consumption of the parent TMDSCB molecules was achieved within the first 30 min for all three samples at these two temperatures. The cross-sectional SEM images of all carburized filaments showed that the thickness of the tungsten carbide layer was increased significantly at temperatures higher than 1800 °C, and the AES depth profile of the three carburized filaments prepared at 2000 °C indicated that the C content quickly reached the terminal level representing the W_2C phase. All these suggest that the carburization of the W filament dominates over the gas-phase reactions at temperatures higher than 1800 °C. This leads to a quick consumption of the source gas molecules and a sharp decrease in the intensities of signals from secondary gas-phase reaction products. Therefore, it is shown here that the gas-phase reactions dominate at $T \leq 1400$ °C. High temperatures favor the carburization of filaments, which in turn reduced the gas-phase reaction rates.

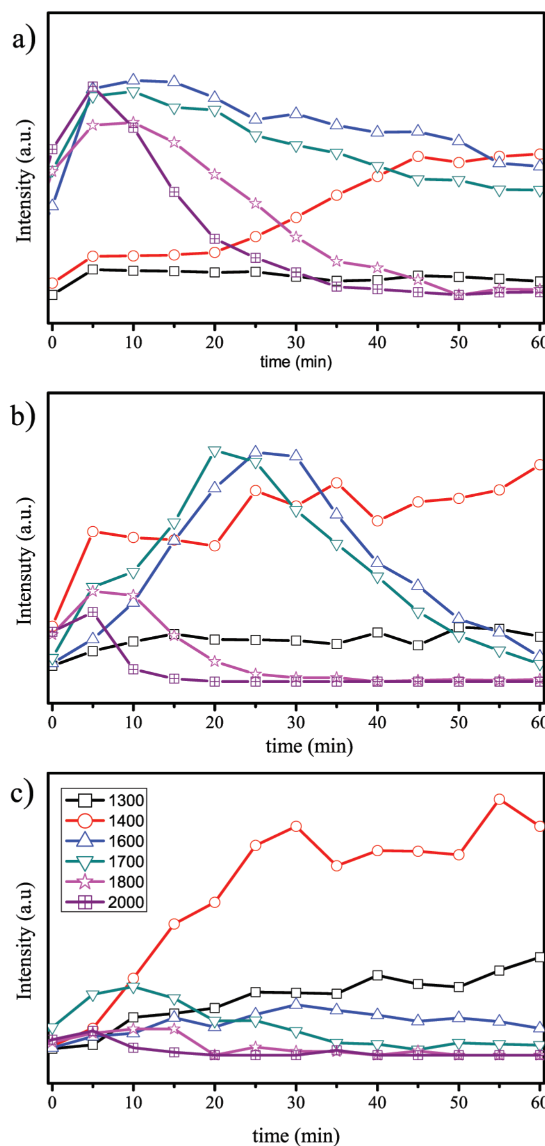

FIGURE 11. Intensity distribution of signals from the 1,3,3-trimethyl-1-ethyl-1,3-disilacyclobutane ion (*m/z* 158) versus filament-on time for (a) 0.48 Torr, (b) 0.24 Torr, and (c) 0.12 Torr of TMDSCB samples at different filament temperatures.

Our study on the carburization process of W filaments with the TMDSCB source gas using SEM/AES, TOF mass

ARTICLE

spectrometry, and power consumption measurements clearly demonstrates that the carburization changes the filament structures, causes a variation in the filament temperatures, leads to a significant increase in the reactant consumption rate, and influences the gas-phase species distribution. Some successes in alleviating the effect of filament carburization have been reported in the literature. These include decarburization from a carburized W filament by heating it at high temperatures ($T \geq 1900$ °C) under vacuum (26, 30, 31) and precarburization of W filaments using a diluted CH_4 in H_2 mixture (32, 33) in the diamond film formation processes using HWCVD. However, the removal of carbon from carburized tungsten via an etching reaction involving hydrogen atoms was not observed in a previous study by Winters et al. (26). This is different from that observed for the silicidized W filaments (7). Further studies are warranted to determine whether heating under vacuum and/or hydrogen etching works for removing carbon from carburized filaments when using TMDSCB as a source gas in a HWCVD reactor.

CONCLUSIONS

Carburization of W filament was observed when using TMDSCB containing both C and Si in a HWCVD reactor. No silicidation was shown to occur. The carburization is mainly caused by the interaction of methyl radicals with the W filament. This agrees well with results from filament carburization in the hot filament assisted CVD of diamond using CH_4/H_2 mixtures. AES analysis of the filament deposits has shown that both WC and W_2C alloys as well as graphite can form on the filament surface, depending on the filament temperatures and source gas pressures. However, both WC and graphite are converted to W_2C when C diffuses into the filament. It is shown that at filament temperatures lower than 2000 °C the thickness of the W_2C layer increases with increasing temperature and partial pressures of TMDSCB samples, suggesting that the evaporation of C atoms from the filament surface is not significant at these temperatures. It has been shown that monitoring the power supplied to the filament in the HWCVD process using TMDSCB source gas provides a good indication of the change in the filament structures and the carburization of filaments. Formation of graphite, WC, and W_2C due to the carburization of filaments causes changes in the consumption rate of the source gas and also intensities of gas-phase reaction products. The interplay between the gas-phase reactions and filament carburization when using TMDSCB in a HWCVD reactor is characterized by the dominance of gas-phase reactions at $T \leq 1400$ °C and of filament carburization at $T \geq 1800$ °C.

Acknowledgment. This work was funded by the National Sciences and Engineering Council of Canada (NSERC), the Canadian Foundation for Innovation, and the University of Calgary. Y.J.S. is grateful for an NSERC University Faculty Award. Access to SEM was kindly provided by the Microscope and Imaging Facility at the University of Calgary and access to AES by the Alberta Center for Surface Engineering and Science at the University of Alberta.

REFERENCES AND NOTES

(1) Mahan, A. H.; Carapella, J.; Nelson, B. P.; Crandall, R. S.; Ballberg, I. *J. Appl. Phys.* **1991**, *69*, 6728–6730.
(2) Matsumura, H. *Appl. Phys. Lett.* **1987**, *51*, 804–805.
(3) Proceedings of the 4th International Conference on Hot-wire CVD (Cat-CVD) Processes. *Thin Solid Films* **2008**, *516* (5).
(4) Holt, J. K.; Swiatek, M.; Goodwin, D. G.; Atwater, H. A. *J. Appl. Phys.* **2002**, *92*, 4803–4808.
(5) Van Veenendaal, P. A. T. T.; Gijzeman, O. L. J.; Rath, J. K.; Schropp, R.E. I. *Thin Solid Films* **2001**, *395*, 194–197.
(6) Honda, K.; Ohdaira, K.; Matsumura, H. *Jpn. J. Appl. Phys.* **2008**, *47*, 3692–3698.
(7) Tong, L.; Sveen, C. E.; Shi, Y. J. *J. Appl. Phys.* **2008**, *103*, 123534-1–123534-6.
(8) Rye, R. R. *J. Appl. Phys.* **1994**, *76*, 1220–1227.
(9) Zeiler, E.; Schwarz, S.; Rosiwal, S. M.; Singer, R. F. *Mater. Sci. Eng., A* **2002**, *335*, 236–245.
(10) Comerford, D. W.; D'Haenens-Johansson, U. F. S.; Smith, J. A.; Ashfold, M. N. R.; Mankelevich, Y. A. *Thin Solid Films* **2008**, *516*, 521–525.
(11) Mahan, A. H. *Solar Energy Mater. Solar Cells* **2003**, *78*, 299–327.
(12) Zhang, Q.; Zhu, M.; Wang, L.; Liu, F. *Thin Solid Films* **2003**, *430*, 50–53.
(13) Shi, Y. J.; Lo, B.; Tong, L.; Li, X.; Eustergerling, B. D.; Sorensen, T. S. *J. Mass Spectrom.* **2007**, *42*, 575–583.
(14) Tong, L.; Shi, Y. J. *Thin Solid Films* **2009**, *517*, 3461–3465.
(15) Li, X. M.; Eustergerling, B. D.; Shi, Y. J. *Int. J. Mass Spectrom.* **2007**, *263*, 233–242.
(16) Sara, R. V. *J. Am. Ceram. Soc.* **1965**, *48*, 251–257.
(17) Baker, H. *Alloy Phase Diagrams*; ASM International: Cleveland, OH, 1992, ASM Handbook Vol. 3, pp 2−115.
(18) Okoli, S.; Haubner, R.; Lux, B. *Surf. Coating Technol.* **1991**, *47*, 585–599.
(19) Schwarz, S.; Rosiwal, S. M.; Frank, M.; Breidt, D.; Singer, R. F. *Diamond Relat. Mater.* **2002**, *11*, 589–595.
(20) Van der Werf, C. H. M.; Van Veenendaal, P. A. T. T.; Van Veen, M. K.; Hardeman, A. J.; Rushce, M. Y. S.; Rath, J. K.; Schropp, R. E. I. *Thin Solid Films* **2003**, *430*, 46–49.
(21) Bakker, R.; Verlaan, V.; Verkerk, A. D.; Van der Werf, C. H. M.; Van Dijk, L.; Rudolph, H.; Rath, J. K.; Schropp, R. E. I. *Thin Solid Films* **2009**, *517*, 3555–3558.
(22) Touloukian, Y. S. *Thermophysical Porperties of High-temperature Solid Materials*; Macmillan: New York, 1967; Vol. 5, pp 205−213.
(23) Martin, L. R.; Hill, M. W. *J. Mater. Sci. Lett.* **1990**, *9*, 621–623.
(24) Chu, C. J.; D'Evelyn, M. P.; Hauge, R. H.; Margrave, J. L. *J. Appl. Phys.* **1991**, *70*, 1695–1705.
(25) Harris, S. J. *Appl. Phys. Lett.* **1990**, *56*, 2298–2300.
(26) Winters, H. F.; Seki, H.; Rye, R. R.; Coltrin, M. E. *J. Appl. Phys.* **1994**, *76*, 1228–1243.
(27) Winters, H. F. *J. Chem. Phys.* **1975**, *62*, 2454–2460.
(28) Winters, H. F. *J. Chem. Phys.* **1976**, *64*, 3495–3500.
(29) Wills, J. B.; Ashfold, M. N. R.; Orr-Ewing, A. J.; Mankelevich, Y. A.; Suetin, N. V. *Diamond Relat. Mater.* **2003**, *12*, 1346–1356.
(30) Andrews, M. R.; Dushman, S. *J. Phys. Chem.* **1925**, *29*, 462–472.
(31) Bague, P.; Morizot, J. P.; Desgardin, G. *J. Phys. D: Appl. Phys.* **1994**, *27*, 402–406.
(32) Menon, P. M.; Edwards, A.; Feigerle, C. S.; Shaw, R. W.; Coffey, D. W.; Heatherly, L.; Clausing, R. E.; Robinson, L.; Glasgow, D. C. *Diamond Relat. Mater.* **1991**, *8*, 101–109.
(33) Smith, J. A.; Cameron, E.; Ashfold, M. N. R.; Mankelevich, Y. A.; Suetin, N. V. *Diamond Relat. Mater.* **2001**, *10*, 358–363.

AM900329Q